Dynamics of Excited Rare-Gas Atoms with Halide Molecules: The Ar(^{3}P) + ClF → ArCl* + F, ArF* + Cl Reaction†

Joan Sogas,‡ Margarita Albertí,*,‡ Xavier Giménez,*,‡,§ and Antonio Aguilar‡

Departament de Química Física and Centre Especial de Recerca en Química Teòrica, Universitat de Barcelona, Martí i Franquès, 1, 08028 Barcelona, Spain, and Department of Chemistry, University of California, Berkeley, Berkeley, California 94720

Received: March 31, 2000; In Final Form: September 7, 2000

The product species originating from the interaction between metastable Ar atoms and the ClF molecules were studied using theoretical (structure and dynamics) methods. Quasiclassical trajectory calculations were carried out on an analytical, monovalued potential energy surface. The energy surface was obtained by means of a fit to CIS (UHF) ab initio points calculated for a set of relevant triatomic configurations, adequately connected to assume that the reaction takes place adiabatically. Cross sections, rate constants, and products' energy disposal for both ArCl* and ArF* excimer formation were calculated, showing a dominancy of the less stable ArCl* + F channel. In addition, angular distributions and rotational alignments for both product channels were analyzed. The influence of reactant internal excitation on integral cross sections and product energy distributions was also studied, considering a wide range of initial rovibrational levels. A remarkable enhancing effect of the reactant rotation was found, as compared to vibration, for the ArCl* product, whereas the opposite trend is observed for the ArF* channel. Whenever possible, the observed behavior was related to both HHL and HLH kinematical considerations. The effect of rotational excitation was used as well to elucidate the angular momentum transfer mechanism among the two competing reaction channels. The role of a relevant rotation−orbiting coupling was identified. Results are found to be, overall, in agreement with the available experimental information, for the title reaction as well as other related systems. This indicates that the fundamental assumption of the present work, namely that the reaction proceeds on a single excited adiabatic potential surface, is accurate enough to account for the main trends of the reaction dynamics.

1. Introduction

The formation of rare-gas halide (Rg*−X) stable molecules has been extensively studied in the past, mainly owing to its relevance to the development of new excimer laser systems.[1] Equally important is the fact that the rare-gas monohalides belong to a chemically interesting group of molecules, since they play an important role in the understanding of the chemical bond.[2,3] For instance, a remarkable feature characterizing the Rg*−X compounds is that they can be easily obtained in different electronic states. This fact creates a fundamental difficulty in the detailed characterization of the related reactive processes.

The available experimental information on rare-gas halide molecules has been produced under both molecular beam and thermal conditions. Aquilanti et al.[4] carried out molecular beam studies of weak open-shell interactions, using an atomic halogen beam in its electronic ground state, which was collided against a rare-gas atom beam. The analysis of the results permitted an accurate characterization of the ground and lower lying excited states of the weakly bound Rg−F* complexes. Other molecular beam experiments[5−12] determined aspects such as cross sections as a function of collision energy and product rotational alignments.[13] Bulk experiments were performed by Setser et al.,[14−20] who derived, from flowing-afterglow studies, the spectroscopic properties, the disposal of available energy into product vibration and the thermal rate constants, for reactions between metastable rare gas atoms and halide molecules (of the type MX, X_2, and XY, where M = CH_3, ... and X,Y = F, Cl, Br, ...). Most of the above experiments have been performed on homonuclear diatomic halogen molecules,[1,3,5−35] information concerning the heteronuclear variant being less frequent.[6,17,36−38] However, as will be seen below, this latter case allows for the possibility of analyzing excimer formation within competing mechanisms, thus providing, in principle, a more complex reactive process.

From the theoretical side, studies on these systems have been hampered by the difficulty of accurately calculating excited electronic states. Consequently, the availability of reliable potential energy surface (PES) is poor. Actually, general predictions on the dynamic behavior can be performed assuming, as is well-known, that the excited states of this kind of molecules are found to be predominantly ionic. Then most of the experiments can be modeled in terms of the strong similarity between the Rg*−X complexes and the alkali halide compounds, which can be considered as prototypic ionic-type species. In particular, collisions between halide molecules with metastable rare-gas atoms are considered to be well understood assuming that crossings from neutral to ionic potential energy curves take place at large internuclear distances. This mechanism explains the large cross sections observed in the excited rare-gas plus halogen reactions, in analogy with the well-known harpooning processes between alkali atoms plus halogen molecules. This enhanced reactive behavior is in strong contrast with the low to null reactivity found for the different rare gases

† Part of the special issue "C. Bradley Moore Festschrift".
‡ Universitat de Barcelona.
§ University of California.

10.1021/jp001228b CCC: $19.00
Published on Web 10/25/2000

in their lowest electronic states. However, as long as a closer inspection to the comparison between the alkali and excited rare-gas reactivity is performed, the limitations of the model manifest in certain discrepancies. For instance, a rather different product energy disposal has been measured. Its theoretical explanation, as may be expected, requires a much more precise knowledge of the potential energy surface and a detailed exploration of the reaction dynamics.

The present work deals with a structural and dynamical theoretical study of the

$$\mathrm{Ar}^*(^3\mathrm{P}) + \mathrm{ClF}(^1\Sigma^+) \rightarrow \mathrm{ArCl}^*(^2\Pi) + \mathrm{F}(^2\mathrm{P}) \rightarrow \mathrm{ArF}^*(^2\Pi) + \mathrm{Cl}(^2\mathrm{P})$$

simultaneous, excited state reactions. Both reaction channels are exoergic, by 1.85 and 2.04 eV, respectively, so that they will compete for product formation. Actually, the main reasons for focusing on these processes are the overall nonstandard reaction conditions. These are given by the excited electronic state, the ionic-type nature of the interaction and the two competing product channels. One would then expect a reaction scattering dynamics showing up fingerprints from the above features. The experimental thermal rate constants for both channels are known,[37] which will be used as a reference to check the reliability of the present study.

To the best of our knowledge, no previous ab initio or dynamics studies are available for the title reaction. Even though general descriptions of ground and excited states of ArF, KrF, and XeF are available,[39] as well as ground and lowest excited states of rare-gas oxides (including comparisons with experiments for the repulsive part of the interaction and features of excited states,[40] and anisotropy function analysis),[41] the lack of structural information on the complete $\mathrm{Ar}^*(^3\mathrm{P}) + \mathrm{ClF}$ system made it necessary to perform ab initio quantum chemistry calculations on it, so as to get the required PES knowledge. These calculations yielded a mesh of ab initio points, which was assumed to scan the relevant region of configuration space. The mesh was then fitted to a simple London−Eyring−Polanyi−Sato (LEPS) functional, and dynamics calculations were performed on it, by means of the standard quasiclassical trajectory (QCT) method. The QCT technique has been chosen because of its usual feasibility, in the early stages of a comprehensive theoretical study for a given chemical reaction. In particular, they are used in the present work, among other purposes, to validate the PES here developed, as well as to gather knowledge on the orientational, alignment and, in general, the angular momentum-related dynamics, features reasonably well described by classical methods. Actually, the three heavy atoms participating in the reaction and the rather featureless PES resulting from the ab initio study give additional support to the accuracy of the QCT technique. Quantum mechanical scattering calculations, at least under some approximations, can also be performed, although they are presently left for future work.

The remainder of the paper is organized as follows: section 2 describes the ab initio calculations and the potential energy surface. Results of the dynamics and their comparison with experiments are given in section 3 and, finally, a summary and conclusions are given in section 4.

2. Potential Energy Surface and Dynamics Calculations

The main purpose of the present study is to analyze the dynamics of both ArCl* and ArF* excimer formation, from the $\mathrm{Ar}^*(^3\mathrm{P}) + \mathrm{ClF}(^1\Sigma^+) \rightarrow \mathrm{ArCl}^*(^2\Pi) + \mathrm{F}(^2\mathrm{P})$, $\mathrm{ArF}^*(^2\Pi) + \mathrm{Cl}(^2\mathrm{P})$ elementary reactions. Since little quantitative data is known about the electronic interaction in the Ar* + ClF system, the first stage of this study deals with the construction of an adequate PES.

Overall trends on the topology of the PES have been obtained through ab initio calculations using the configuration interaction singles (CIS)[42] methodology, at the UHF/6-311+G(df) level, as implemented in the Gaussian 94 program package.[43] A reasonable accuracy from the CIS calculations is expected, since our interest focuses on the first excited state coming from the single excitation of the Ar atom.[44] The relevant region of the tridimensional configuration space was explored as follows: a mesh of ab initio points was obtained as a function of the internuclear distances. This mesh was built up from the geometries obtained by considering a set of fixed orientation angles and then, for each angle, varying the two internuclear distances.

Owing to the specifics of the electronic interaction in the ArClF* system, a large number of states may be involved in collisional processes. The complete multisurface problem appears unaffordably involved, with the present availability of experimental and theoretical information. Because of that, our first trial consists in generating a reasonable single adiabatic PES, for the metastable excited state. Given this, the main difficulty originates from the actual choice of the excited state from the whole set provided by the CIS calculations. This state must correlate asymptotically to the ^{3}P state of the rare gas. Thus, the energies were picked up checking, for each triatom's geometrical configuration, that the excited state corresponds to that of the Ar atom. A further check consisted in confirming that the selected points led to the least change in charge distribution and dipole moment. This procedure yielded a set of ^{3}A′ symmetry points, correlating asymptotically to the proper electronic states of reactants and products.

The comparison of the resulting dynamical data with experimental information might be, nevertheless, somewhat controversial. This is so since some contradiction exists about the relative energy ordering of the excited RgX B and C states. On one hand, Gundel et al.[14] performed an estimation of the ArCl* diatomic potentials, obtaining a $^2\Pi$ state lying lower in energy than the $^2\Sigma$, although both curves were certainly rather close. Instead, Liegel et al.[26] deduced from experiments an opposite ordering. Furthermore, the experimental rate constants referred to in the present work[37] do not distinguish among the B and C states, since it is provided a unique, global rate constant value. Given this uncertainty and the small energy gap between both B and C states, in the present work it has been chosen to label the ArX* states as $^2\Pi$, since it is the excited state actually picked from our calculations (the noncollinear asymptotes leading to an electron in a perpendicular π orbital). In conclusion, given the focus of the present study on averaged quantities, any result will be considered to equally apply to B and/or C RgX states. Thus, no efforts are presently made to distinguish among the possible differences in the dynamics, in particular those involving the angular aspects.

Results show a marked ionic character for the Ar* + ClF interaction, in agreement with previous results for alkali-metastable rare-gas atom systems. Other important PES features are the barrierless collinear minimum energy reaction paths, for both the ArCl* and ArF* channels, as well as the absence of any minima on the PES. The barrierless approach was previously found to characterize the Xe* + ICl and the Xe* + IBr processes,[6,45] for which a typically decaying cross section as a function of energy was measured.

TABLE 1: LEPS PES Diatomic Constants and Sato Parameters Used in the Present Work

	D_e/eV	R_e/Å	α/Å^{-1}	S
ClF	2.666	1.6283	2.2905	0.125
ArCl	4.510	2.7702	0.7002	0.150
ArF	4.702	2.4000	0.88125	0.330

The rather featureless mesh provided by the CIS ab initio points, along with the collinear minimum energy path (MEP), suggests the possibility of using a simple LEPS[46] PES to fit the raw data. This has been our choice. However, it was obtained through a nonstandard process, due to a lack of consistency in the diatomic dissociation limits.

Thus, it was obtained that the excited state mesh of ab initio points led to ionic dissociation limits for both the ArCl and ArF diatomic partners. Specifically, both molecules dissociate to the ground ionic states, $Ar^+(^2P)$, $Cl^-(^1S)$, and $F^-(^1S)$. This is not consistent with the available information for the ClF molecule, since it adiabatically dissociates to the neutral $Cl(^2P)$ + $F(^2P)$ limit. Consequently, some kind of correction was needed. To that purpose, the following procedure was chosen: first, the ab initio data for both ArCl and ArF regions was fitted to an extended Rydberg functional, since it allows a direct reproduction of the ab initio force constants. Then, the diatomic curves were scaled by changing the dissociation limit to that corresponding to the (lower lying) neutral atoms. This procedure yields, in practice, diatomic curves in agreement with the ab initio points up to ca. 5 Å, whereas for higher distances they smoothly switch to the neutral dissociation limit.

Afterwards, the extended Rydberg curves were best fitted to Morse functionals, so as to provide adequate input data for the LEPS function. This global procedure ensures a best reproduction of both force constants and dissociation energies, which could not otherwise be guaranteed through direct use of Morse functions. As for the ClF diatom, a previously fitted potential was used.[47]

The above process is ultimately sensible since it provides a simple way to combine the previous data on ClF with the excited state ab initio data here reported. Further justification comes from the fact that the collision energies considered in the present study are well below both the real and the modified dissociation limits. A final argument, supporting our choice, is that the modifications should be less relevant when comparing to experiments based on excimer formation through electron jump, as in the present case, since it directly leads to dissociating charge-transfer ionic species and so only the ionic part of the PES is probed.[48] On the other hand, a fully consistent ab initio treatment would require a much larger mesh of computed points. This is an expensive task, which might be worthwhile as soon as more detailed experimental information will become available on the title reaction.

Finally, the remaining LEPS Sato parameters have been determined, by trial and error, to best reproduce the experimental branching ratios, through QCT calculations. The resulting analytical PES predicts a barrierless collinear MEP when the Ar atom approaches the Cl end of the ClF diatom, whereas a 0.015 eV barrier is obtained for the collinear Ar−FCl MEP. This small barrier is not present in our ab initio study. However, further fits attempting to eliminate the barrier led to unexpectedly wrong branching ratios. At first sight, these discrepancies may reflect a lack of flexibility of the LEPS PES to properly reproduce the structural features. Nevertheless, one has to consider that the accuracy of the raw ab initio data is, quite probably, lower than the fitted barrier height. More importantly, the remaining dynamical results, as will be shown below, are

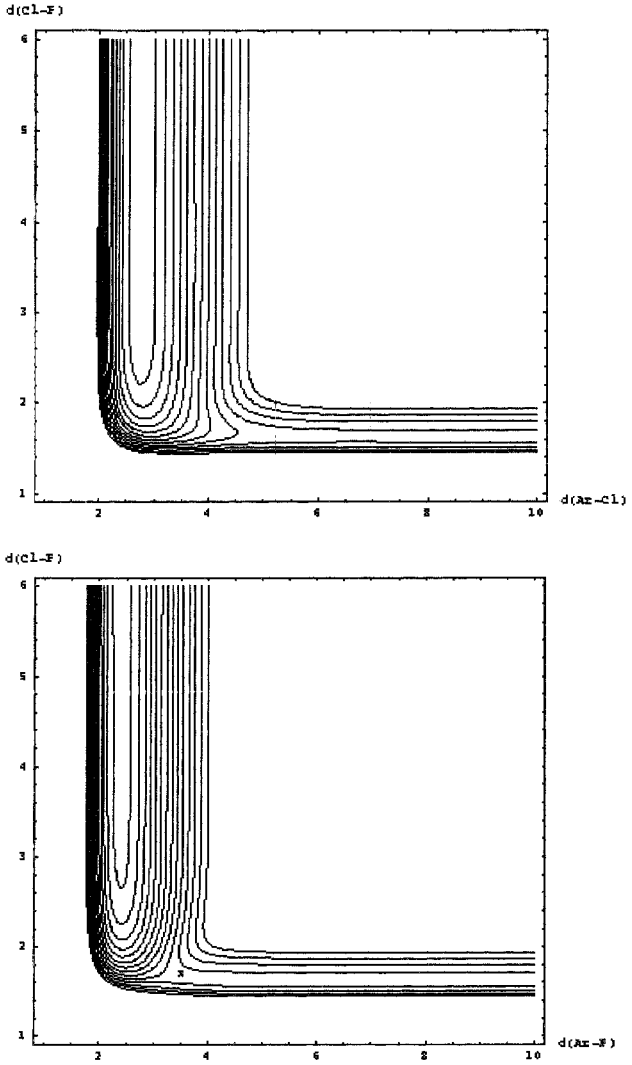

Figure 1. (a, top) PES contour map showing the Ar*−ClF collinear approach. The lowest energy contour corresponds to −4.4 eV, the contour interval being 0.2 eV. Internuclear distances are given in Å. (b) PES contour map showing the Ar*−FCl collinear approach. The lowest energy contour corresponds to −4.6 eV, the contour interval being 0.2 eV. The position of energy barrier is also shown. Internuclear distances are given in Å.

in fairly good agreement with experiments. Thus, it seemed reasonable to keep the original fit, as it provides an overall reliable and simple one-surface dynamical description of the title reactions. Table 1 lists the final set of LEPS parameters, whereas Figure 1 shows the potential energy contours for the Ar* + ClF → ArCl* + F (Figure 1a) and Ar* + ClF → ArF* + Cl (Figure 1b) reaction channels.

Dynamical calculations, on the resulting analytical PES, have been performed for selected initial states, by means of the standard QCT method.[49,50] In particular, the 0.02−0.12 eV translational energy range has been explored from 300 K thermal conditions. In addition, the influence of vibration and rotation has been studied, considering the $v = 0$, 1 and 2, as well as the $J = 0$, 3, 7, 10, 14, 18, 21, 25, 30, 35, and 40 states. For each initial condition, good statistics were obtained running 25 000 trajectories.

3. Results

3.1. Partial and Total Reaction Cross Sections and Thermal Rate Constants. Figure 2 shows the cross section as

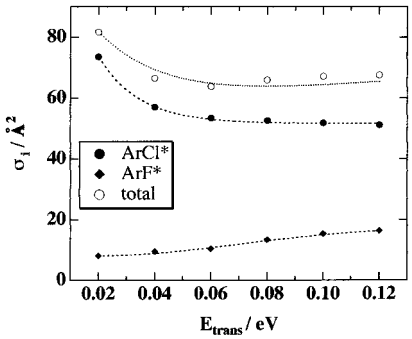

Figure 2. Total and partial reaction cross sections, σ_i (i = ArCl*, ArF*), as a function of reactant translational energy, for the (0,14) reactant rovibrational level. Continuous lines are provided as a guide to the eye only.

a function of collision energy, for both ArCl* and ArF* product channels. They have been calculated for the most populated rovibrational level at 300 K, namely $(v,J) = (0,14)$. Results are consistent with the PES topography, i.e., a decreasing trend for ArCl* and a slightly increasing trend for ArF*. Remarkably, the less stable ArCl* channel clearly dominates in the scanned energy range. The favored formation of the Cl channel has been observed previously in other Rg* + ClF and Rg* + ICl reactions.[18] As for the total cross section, also shown in Figure 2, a qualitatively similar trend has been observed for the Xe* + IBr process,[10] thus showing an increase in the relative production of the lighter halogen at higher energies. On the other hand, this increase at higher energies has not been observed for the Xe* + Br_2 reaction[51] and, in general, in orbiting controlled harpooning mechanisms. Interestingly, the harpooning mechanism predictions, as it is well-known, correctly reproduce the low-energy behavior, but fail to predict the high-energy cross section increase.

Thermal rate constants, for both reaction channels, have been calculated at 300 K. According to the standard formula,[52] the values $k_{ArCl^*} = 33.65 \times 10^{-11}$ cm^3 s^{-1} and $k_{ArF^*} = 5.17 \times 10^{-11}$ cm^3 s^{-1} have been obtained, which have to be compared with Setser and Kolts's measurements.[37] They provide the values 38.0 $\times 10^{-11}$ cm^3 s^{-1} and 2.9 $\times 10^{-11}$ cm^3 s^{-1} for k_{ArCl^*} and k_{ArF^*}, respectively. As stated previously, these values have been the best fits to the experimental data, as provided by the LEPS function used in the present work.

3.2. Products Energy Disposal. Our detailed dynamical characterization of the processes involved in the title reaction begins with the products energy disposal. Figure 3 shows the products energy distribution, as a function of translational energy, for both reaction channels. A large amount of internal excitation is obtained in both cases. This is consistent with the early energy barrier or the early release of electronic energy for the ArF* + Cl and ArCl* + F channels, respectively. These results are also in agreement with related experimental information. In particular, Kolts et al.[18] measured, for the XeCl product, vibrational excitations to be, approximately, 77% and 71% of available energy, in the Xe* + Cl_2 and Xe* + ClF reactions, respectively.

Comparison between both channels reveals a higher degree of overall internal excitation for ArCl* + F. However, product rotation is higher for ArF* + Cl. The product energy dependence on collision energy shows, for ArCl* + F, an essentially constant dependence for vibration and an increase of rotation with increasing energy, whereas the ArF* + Cl channel leads to a clear increase in vibrational content and a diminution in product rotation.

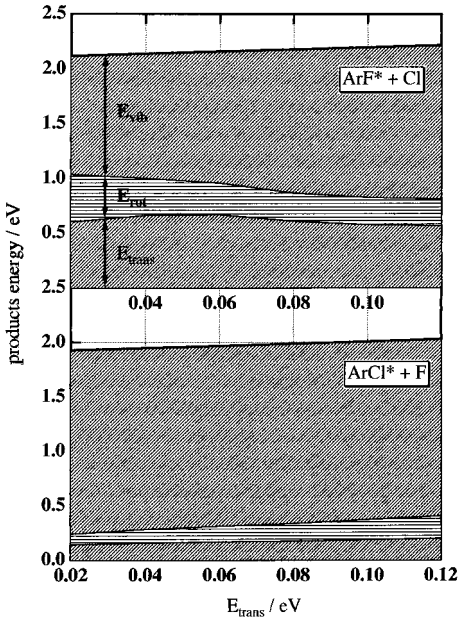

Figure 3. Product energy distribution as a function of reactant translational energy, for the ArCl* + F channel (lower panel) and the ArF* + Cl channel (upper). Each trace is built adding its contribution to the previous one (stacked plot).

An explanation for the above behavior requires considering additional information. In particular, it will prove convenient to analyze quantities related to the angular motion, such as rotational alignments and angular distributions, whose results are shown next.

3.3. Alignment Effects. The determination of the vector properties is known to provide interesting insights on the scattering dynamics. For the present system, in addition, these quantities are of relevance for the detailed characterization of the product molecules as excimer lasers.

Figure 3 shows that rotational and translational energy increase linearly with reactants translational energy, for the ArCl* + F channel. In addition, it has been previously stated that the PES is rather featureless. Consequently, a kinematic analysis appears to be relevant. As is well-known,[52] the angular momentum transfer may be properly analyzed in terms of the reactants masses, a relevant parameter being $\cos^2\beta = m_A m_C/(m_B + m_C)(m_A + m_B)$. For Ar* + ClF → ArCl* + F, $\cos^2\beta = 0.1824$ so that it might be expected the relations $\mathbf{J}' \sim \mathbf{L}$ and $\mathbf{L}' \sim \mathbf{J}$ to approximately hold, which is a typical behavior for heavy−heavy−light (HHL) systems (from hereon, bold quantities correspond to rotational (**J**) and orbital (**L**) angular momentum vectors, whereas primed quantites refer to product states and nonprimed to reactants). Then, it is easy to show that these angular momenta correlation schemes lead to a linear dependence of E'_{rot} on E_{trans}. This is in agreement with the present QCT results. This kind of dependence can be used as an indicator of product orbital angular momentum constancy,[53] being the basis for the constant product orbital angular momentum (CPOAM) model.[53−56] This model, in turn, leads to a simplified way of calculating the rotational alignments. They describe the orientation of the rotational angular momentum vector $\mathbf{J}'$ with respect to the initial velocity vector $\mathbf{k}$, being usually given as the Legendre second moment $P_2\langle \mathbf{J}'\cdot\mathbf{k}\rangle$ of the products angular distribution.

The rotational alignments have been calculated from the CPOAM model,[57] using the present QCT calculations as source data.[54] They are shown in Figure 4 and found to lie only slightly below the kinematic HHL limit, $P_2\langle \mathbf{J}'\cdot\mathbf{k}\rangle = -0.5$. This result

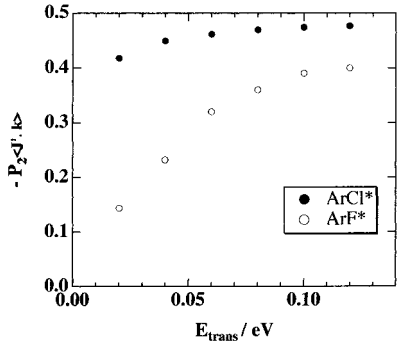

Figure 4. Rotational alignments for the (0,14) reactant rovibrational level, as a function of reactant translational energy, for both reaction products.

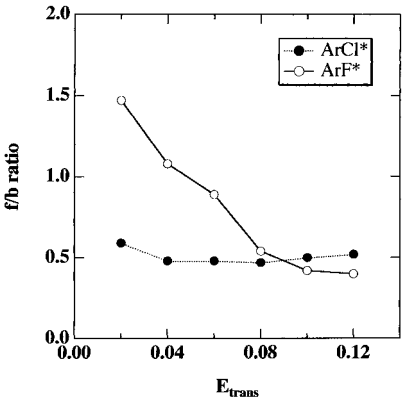

Figure 5. Forward/Backward ratio as a function of translational energy, for the (0,14) reactant rovibrational level, for both product channels.

is in agreement with that found in other reactive processes involving excited rare gas atoms and halogen molecules, in particular those corresponding to the Rg*−X formation in reactions between rare-gas and XH (X = F, Cl, Br, I) molecules.

On the other hand, the Ar* + ClF → ArF* + Cl channel leads to a value of $\cos^2\beta = 0.4413$. Then, a transfer mechanism from **L** to both **J′** and **L′**, with the maximum alignments lying well below the kinematic limit, should be expected. Figure 4 confirms the expectations for the rotational alignments, this result being comparable to that obtained in reactions between rare-gas and X_2 molecules, namely processes for which the kinematic constraints are smaller.

Actually, the product internal energy disposal for the ArF* + Cl product channel could be analyzed, in terms of mass combination, as that determined by a heavy−light−heavy (HLH) case. It is well-known[58] that smaller skew angles lead, for similar PES, to larger degrees of vibrational excitation. This is in contradiction with the present results. However, a change is observed in the transition state (TS) position when changing from ArCl* + F to ArF* + Cl (i.e., from HHL to HLH). Consequently, the trend in product vibrational excitation can be different. This appears to be the case in the present work. Inspection of Figure 1 reveals a more delayed position of the ArF* TS with respect to that for ArCl*. The final outcome, a minor product vibrational energy content for ArF* than for ArCl*, results then from a larger effect of the TS position than the change in mass combination. Nevertheless, the partial HLH nature of the ArF* + Cl product contributes, along with the more delayed TS position (although, in absolute terms, still an early one), to a higher degree of reactivity enhancement, by reactant vibrational excitation, for ArF* than for ArCl*.

3.4. Angular Distribution. Information concerning the spatial aspects of this competitive process can be gained from an analysis of the angular distributions. We have found particularly useful the plot of the forward/backward (f/b) scattering ratio as a function of translational energy, which is shown, for both reaction channels, in Figure 5.

Results for the ArCl* + F channel show that this ratio is about 0.5 and nearly independent of E_{trans}. This means that $^2/_3$ of total reactive trajectories leading to ArCl* are scattered on the backward hemisphere. Thus, the collision mechanism is dominated by collinear, head-on impacts, for low impact parameters, whereas the contribution to reaction of trajectories with larger impact parameters leads to the ca. $^1/_3$ of forward scattering.

On the other hand, for ArF* + Cl products it is observed that the f/b ratio varies sharply from high (∼1.5) to low (∼0.5) values as energy is increased. This strong dependence suggests a change of the reaction mechanism with translational energy. This possibility has been checked analyzing individual trajectories. It has been found, at low energies, that there is an important contribution from nondirect trajectories, proceeding through the Cl end. These contributions lead to forward scattering since, owing to the larger Cl size, large impact parameters are necessary for these collisions to occur. As energy is increased, an increasingly larger contribution of direct, collinear collisions has been found, leading to a decrease of the f/b ratio.

This behavior explains the large dominance of ArCl* product formation al low energies, even though it is the less stable of the two possible product molecules. This provides insight on the competitive mechanisms between both channels. It seems reasonable to state, from the above results, that ArCl* product formation is preferred owing to, essentially, two factors. On one hand, the greater size of the Cl atom and the marked isotropy of the PES for ArCl* + F leads to a major facility for these reactive collisions to take place. This combines with the fact that the PES leading to ArF* + Cl formation is much more anisotropic, i.e., orientation-selective, and the F-atom size is smaller.

3.5. Effect of Internal Energy Excitation. Interesting effects on the reaction dynamics of the title reactions are obtained upon increase of either rotational or vibrational energy. A rather complete study has been performed, considering, as indicated previously, an ample range of initial (v,J) levels.

(i) Effect on Reaction Cross Sections. (*a*) *Of Reactant Rotation.* the cross section dependence on rotation (Figure 6a) is an increase for ArCl* but a decrease for ArF*, which is consistent with the degree of anisotropy[59,60] (low and high, respectively) of each PES. The detailed dependence with J is nonmonotonic: σ_{ArCl^*} initially increases, goes through a maximum at about $J = 25$ and then decreases, whereas σ_{ArF^*} first decreases, takes a minimum value at about $J = 10$, then increases up to a shallow maximum at $J \sim 25$ and finally it smoothly decreases. Rather noticeable is the cross section increase at intermediate J values, for ArF*. The previous decline, caused by the PES anisotropy, is attributable to the lesser availability of favorable configurations. However, the subsequent increase is due to the fact that, as the rotational speed increases, the favorable configurations become available a higher number of times for the same collision energy and thus the chance of encountering the right configuration for reaction increases.[60]

(*b*) *Of Reactant Vibration*. The cross section dependence on vibration (Figure 6b) is monotonic for both reaction channels. Actually, an essentially linear dependence is obtained in all cases, with positive slopes, even those considering excited reactant rotational states. The enhancement rate, in relative

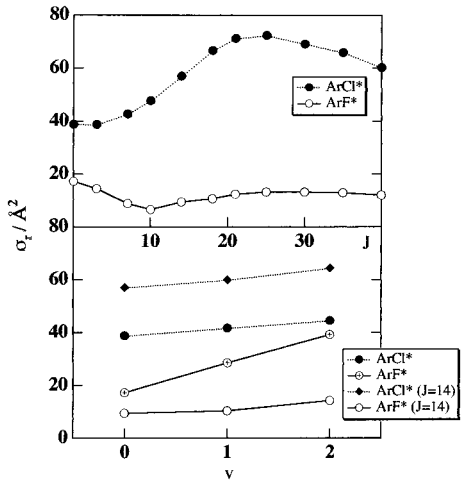

Figure 6. (a, upper panel) Reaction cross section as a function of the reactants rotational quantum number J, at a translational energy of 0.04 eV. All states correspond to $v = 0$. (b, lower panel) Reaction cross section as a function of the reactants vibrational quantum number v, at a translational energy of 0.04 eV. $J = 0$ and $J = 14$ cases shown.

TABLE 2: ArCl* + F Energy Distribution, at $E_{trans} = 0.04$ eV, for Different Initial Rovibrational Levels[a]

v, J	E_{acc}/eV	E'_{vib}/eV	E'_{rot}/eV	E'_{trans}/eV
0, 0	1.933	1.7 (89)	0.1 (5)	0.1 (6)
1, 0	2.030	1.8 (88)	0.1 (5)	0.1 (7)
2, 0	2.127	1.9 (88)	0.1 (5)	0.1 (7)
0, 14	1.946	1.7 (85)	0.1 (7)	0.2 (8)
1, 14	2.043	1.8 (86)	0.1 (6)	0.2 (8)
2, 14	2.140	1.8 (86)	0.1 (6)	0.2 (8)

[a] Results in parentheses correspond to percentage of accessible energy.

TABLE 3: ArF* + Cl Energy Distribution, at $E_{trans} = 0.04$ eV, for Different Initial Rovibrational Levels[a]

v, J	E_{acc}/eV	E'_{vib}/eV	E'_{rot}/eV	E'_{trans}/eV
0, 0	2.125	1.7 (78)	0.1 (4)	0.4 (18)
1, 0	2.222	1.8 (81)	0.1(3)	0.4 (16)
2, 0	2.319	1.9 (82)	0.1 (4)	0.3 (14)
0, 14	2.138	1.1 (53)	0.3 (16)	0.7 (31)
1, 14	2.235	1.2 (56)	0.3 (13)	0.7 (31)
2, 14	2.332	1.4 (61)	0.2 (11)	0.7 (28)

[a] Results in parentheses correspond to percentage of accessible energy.

terms, is higher for ArF* than for ArCl*. It reflects, as pointed out above, the HLH character and the more delayed barrier of the ArF* + Cl product channel.

In conclusion, it is found that a similar amount of energy, put either in rotation or in vibration, causes an opposite effect depending on the reaction channel. Rotation is remarkably much more effective than vibration for ArCl*, but the opposite is true, namely vibration is much more effective than rotation (actually, the latter inhibits reactivity), for ArF*. It clearly results, as stated, from the combined effect of the low and high degree of anisotropy and the partial HHL and HLH nature, respectively, of each reaction channel.

(ii) Effect on Product Energy Distributions. The present study has been completed analyzing the dependence of product energy distributions on reactant internal energy. Tables2 and 3 show these results, which correspond, respectively, to the ArCl* + F and the ArF* + Cl channels.

As for ArCl* + F, an increase in reactants vibrational energy does not substantially alter the relative product energy distribution, this result being valid independently of the initial rotational excitation. These facts evidence the major influence of the collinear head-on collisions and the HHL kinematical constraint.

The same results for ArF* + Cl show some differences. First, initial vibration causes an increase in both absolute and relative quantities for product vibration. Second, a major change is found when going from $J = 0$ to $J = 14$ initial states. However, this influence of rotation is found to be less simple, when considered in detail, so as to deserve a separate analysis.

TABLE 4: Product Rotational Energy and Products Mean J Value ($\langle J' \rangle$), for Both Reaction Channels, at $E_{trans} = 0.04$ eV and $v = 0$[a]

J	E'_{rot}(ArCl*)/eV	E'_{rot}(ArF*)/eV	$\langle J' \rangle_{ArCl*}$	$\langle J' \rangle_{ArF*}$
0	0.1 (5)	0.1 (4)	81	52
3	0.1 (5)	0.1 (5)	82	61
7	0.1 (5)	0.2 (8)	84	79
10	0.1 (6)	0.3 (13)	89	100
14	0.1 (7)	0.3 (16)	94	108
18	0.1 (7)	0.3 (16)	95	109
21	0.1 (7)	0.4 (17)	96	114
25	0.1 (7)	0.4 (17)	98	115
30	0.1 (7)	0.4 (19)	102	122
35	0.2 (8)	0.5 (22)	105	132
40	0.2 (9)	0.6 (25)	110	140

[a] Results in parentheses correspond to percentage of accessible energy.

(iii) Effect of Reactant Rotation on Product Rotation. As stated, the effect of reactant rotation on product rotational distributions and, in particular, on the mean product rotational energy is rather cumbersome. Table 4 shows the amount of product rotation as a function of initial J, for both reaction channels. Overall, an increase is observed in the product rotational energy as J is increased. However, the enhancement rate is much larger for ArF* + Cl than for ArCl* + F. This is in agreement again with the smaller HHL kinematical constraining (or, equivalently, the larger HLH fulfillment) for the former product channel.

Even though the enhancement rate is larger for ArF* than for ArCl*, the amount of product rotation obtained for very small J is larger for ArCl* ($J = 0$ the low-J case reported in Table 4). For this limiting case, the product angular momentum is exclusively channeled from L. Then, the J' value is determined, on one hand, by the effectiveness in the HHL L to J' transfer, which is larger for ArCl*, but also by the range of L values effective for reaction. A clue for gaining knowledge on this L range is obtained from the f/b ratio, for the specific $(v,J) = (0,0)$ conditions. At $E_{trans} = 0.04$ eV (the same conditions as in Table 4), it is found to be 0.09 and 0.26 for ArF* + Cl and ArCl* + F, respectively. Thus, the stronger backward character for collisions leading to ArF* + Cl points toward a narrower L range. In conclusion, both the smaller HHL constraint or, equivalently, the stronger HLH character, which is well-known to favor a $J \sim J'$ transfer,[61] as well as the smaller initial L effective to reaction, justify the smaller product rotational energy for the $(v,J) = (0,0)$ collisions leading to ArF* + Cl. Nevertheless, even though ArF* + Cl is closer to the HLH mass combination, it does not fully belong to this limiting case, in view of the heavy-to-light mass ratio. This fact helps explaining the observed deviation from the pure $J \sim J'$ channeling.

The detailed dependence of $\langle J' \rangle$ on J provides additional interesting insights on the scattering dynamics of the title reactions. This dependence is plotted in Figure 7. Remarkably, two kinds of dependences are identified. The first one, for low J values (ca. 0−10), is an approximate linear dependence for both channels, with a larger slope for ArF* + Cl. The second, for higher L values (ca. 15−40), is again a linear dependence, less steeper than in the former case and more similar for both

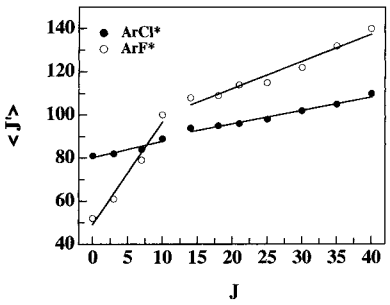

Figure 7. Mean products rotational quantum number as a function of the reactants rotational quantum number, for both reaction channels. Straight lines show the best linear fittings in the $J = 0-10$ and $J = 15-40$ regions.

reaction channels. The interesting fact is that a product channel independence, in the onset of the switching among linear dependences, is found. It strongly suggests that it is due to a local, reactant channel effect, so that it necessarily originates in a local transfer from rotation to either vibration or orbital angular momentum. Our next analysis strongly points toward the second case, i.e., that a rotation-orbiting coupling, along with its change as reactants rotation is increased, is the responsible mechanism for the observed behavior.

Our analysis begins pointing out that, formerly, we have shown that the effect of reactants vibrational excitation on product energy distributions is weak (Tables 2 and 3). This result is valid for both reaction channels, as well as for collisions starting at either $J = 0$ or $J = 14$. This latter behavior tells that no observable effect might be obtained in the case that a reactant's rotational to vibrational energy transfer takes place at high J values. This conclusion is in contradiction with the present results.

Consequently, some kind of rotation−orbiting coupling appears to take place. Transfer between rotational and orbital angular momentum, in either direction, takes place thanks to the potential anisotropy, i.e., through gradients along the adequate angular distance. It is then more likely as the total energy is lower and, in particular, as rotational energy is lower. The reorienting effect is gradually lost owing to the potential averaging effect of increasing rotation. Thus, the local transfer among angular momenta is hampered by an increase of rotational energy. Since the present QCT collisions are characterized by large mean orbital angular momentum values, results can be interpreted considering that, at low rotational energies, an appreciable transfer from orbiting to rotation takes place. This mechanism explains the large slopes obtained in the low-J fittings for the $\langle J' \rangle$ dependence on J. The rotation−orbiting coupling is, according to our present knowledge of the PES, essentially due to the anisotropy of the ArF* + Cl channel. In particular, the inelastic part right before the TS, i.e., the region, still in the reactants channel, where the ArF* + Cl features are begun to be felt, might be the PES portion which provides the physical ingredients for the rotation to orbiting transfer.

As rotational energy is increased, the orbiting to rotation transfer gradually diminishes, as stated. This has an effect which explains some of the features reported in the present work:

(a) On one hand, this behavior is consistent with the previously reported cross section decrease as a function of J, for sufficiently high J, observed for ArCl* + F and, less intense, for ArF* + Cl (Figure 6a). The explanation goes as follows. As the orbiting to rotation transfer diminishes with increasing J, the effective L value increases. This, in turn, may reflect in either an increase in velocity (kinetic energy) and/or impact parameter. The present QCT data show that, in going from low to high J, mean impact parameters are almost unaltered for ArCl* + F (from 4.02 Å for $J = 14$ to 3.88 Å for $J = 40$), but appreciably increase for ArF* + Cl (from 4.05 Å for $J = 14$ to $J = 4.78$ for $J = 40$). This means that, for ArCl* + F, an increase in L goes to an increase in reactants velocity, so that the cross section behaves in the same way than increasing translational energy, for ArCl* + F. For ArF* + Cl, on the other hand, the behavior is mixed. Inspection of Figure 2 confirms that increasing energy (and then increasing rotation) decreases the cross section, for ArCl* + F, whereas a milder effect is obtained for ArF* + Cl.

(b) On the other hand, the $\langle J' \rangle$ dependence on J is milder in the high-J region. This results from the weaker rotation−orbiting inelastic coupling and thus from a more kinematic nature of the collision, for both product channels.

The mean impact parameter behavior as a function of J is a key concept in the previous analysis, but it has been introduced from our raw data, i.e., without any physical intuitive interpretation. Interestingly, it can be easily interpreted in terms of a simple rotor dynamics. In ClF, the center of mass is displaced toward the Cl end. Thus, rotational motion can be described as an F-atom precession around Cl, the latter describing a smaller circle around the center of mass. In other words, the F atom rotates around the "exterior", while Cl is kept more "interior", this effect being much more pronounced as the rotational velocity is higher. In addition, the ClF chemical bond is rather loose, so that centrifugal distortion causes the bond length to increase with rotational energy. The overall effect is that the F atom is mainly in the exterior region, which is larger as rotation is increased, whereas the Cl atom, on the contrary, is mainly in the interior and thus less affected by centrifugal distortion. This causes an increase of the mean impact parameter for ArF* + Cl production and a rough insensitivity for ArCl* + F.

A similar kind of argument has been used for several years to explain the influence of initial rotation on state-selected cross sections for the F + HD → FH(D) + D(H) simultaneous reactions.[62] Results from these studies are found to be in apparent contradiction with the present study. In particular, it is stated that the increasing screening effect, with initial J, of the H atom in the HD rotating molecule, leads to a mild reactivity inhibition when forming FD, whereas enhancement is obtained for FH.

Our results tell, on the contrary, that an enhancement is obtained for the heaviest product channel, while inhibition results from the lightest. An explanation for this behavior might be based on two features. First, it is the fact that, contrary to what happens for the F+HD case, an *important* change in the PES topography is associated to the change from ArCl* to ArF*. The former is, as stated, basically isotropic and purely attractive, whereas the latter is fairly anisotropic and more repulsive. These features link the influence of initial rotation to an enhancing energetic factor and an inhibiting orientational effect, respectively, as previously discussed.

A second argument is that the screening effect, for the specific ClF molecule, has in turn two distinctive features when compared with HD. First of all, the atom rotational velocity is, for the same rotation quantum number J, much lower in our case, due to the heavier masses. Then the screening effectivity is smaller. Second, the Cl-atom size is larger than that of the F atom. This feature, along with the larger Ar−Cl equilibrium distance, contributes to a further diminution of the screening effect, since less penetration is necessary for the Ar−Cl product molecule to be formed.

Thus, to summarize, the apparent discrepancy between the F + HD and the Ar + ClF cases is essentially attributable to both the much higher influence of the PES topography and the smaller role of the screening effect, found for the latter with respect to the former.

4. Summary and Conclusions

In this paper, the dynamics of the Ar* + ClF reaction has been studied by means of the QCT method, using a single-valued LEPS empirical surface where the reaction is assumed to take place adiabatically. Thus, an excited state scattering dynamics, where two product channels are available to reaction, has been explored. The analytical function has been fitted to ab initio results, which follow from considering the collision to asymptotically start on a diabatic covalent surface that later crosses the diabatic ionic potential, transferring an electron. The total reactive cross-section first falls and then smoothly increases, as a function of reactant translational energy. This behavior arises from a dominating decaying law, for the less stable ArCl* product formation, plus an increasing trend for ArF* production, being easily explained from topographical PES considerations. Results are found to agree with other reactions between rare-gas and dihalogen molecules.

In agreement with related experimental observations, the calculations predict a strong internal excitation for both excimers, being higher for ArCl*, for which a high content of vibrational excitation has been found. Results of product rotational alignments show that ArCl* has a higher level of rotational alignment than ArF*. These results are consistent with HHL and HLH kinematic considerations.

The product angular distribution is shown to be independent of E_{trans} and consistent with a dominating collinear, head-on reaction mechanism for ArCl* + F. On the other hand, results corresponding to the ArF* + Cl products suggest a change from a nondirect to a direct reaction mechanism as E_{trans} is increased, which has been confirmed by individual inspection of selected trajectories.

The analysis of the influence of reactant internal excitation on reactivity shows that an increase of internal excitation enhances the reactivity, except for rotational excitation and the ArF* + Cl product. Conversely, rotation is much more effective than vibration for ArCl* + F. Remarkably, the cross section dependence on rotation is nonmonotonic for both reaction channels. These facts have been explained on the basis of kinematic constraints, energy considerations, and the existence of a nonnegligible $\mathbf{L}-\mathbf{J}$ coupling and its change as rotational energy is increased. A simple rotor dynamics is used to interpret the impact parameter dependence on reactant rotation.

On the overall, results seem to indicate that the single-valued surface, constructed taking into account the main characteristics of the reaction mode observed for similar reactions, is able to describe the dynamics of ArCl* and ArF* excimer formation in the $Ar(^3P)$ + ClF colliding system.

Acknowledgment. This work has been supported by the Spanish DGICYT (Project PB97-0919) an the Generalitat de Catalunya (CUR 1998SGR-00008). J.S. also thanks the Spanish MEC for the Predoctoral grant associated with the PB97-0919 Research Project. X.G. acknowledges the Spanish MEC for a "Formación y Mobilidad de Profesorado Universitario" fellowship, and Professor William H. Miller for his kind hospitality.

References and Notes

(1) Kosmas, A. M. *Il Nuovo Cimento* **1984**, *3*, 981, and references therein.
(2) Aquilanti, V.; Cappelletti, D.; Lorent, V.; Luzzatti, E.; Pirani, F. *J. Phys. Chem.* **1993**, *97*, 2063.
(3) Brau, C. A.; Ewing, J. J. *J. Chem. Phys.* **1975**, *63*, 4640.
(4) Aquilanti, V.; Luzzatti, E.; Pirani, F.; Volpi, G. G. *J. Chem. Phys.* **1988**, *89*, 6165.
(5) Rettner, C. T.; Simons, J. P. *Chem. Phys. Lett.* **1978**, *59*, 179.
(6) Hennessy, R. J.; Ono, Y.; Simons, J. P. *Mol. Phys.* **1981**, *43*, 181.
(7) Simons, J. P. *Chem. Phys. Lett.* **1982**, *91*, 484.
(8) Johnson, K.; Paese, R.; Simons, J. P. *Mol. Phys.* **1984**, *52*, 955.
(9) Johnson, K.; Paese, R.; Simons, J. P.; Smith, P. A.; Kvaran, A. *J. Chem. Soc., Faraday Trans.* **1986**, *82*, 1281.
(10) de Vries, M. S.; Tyndall, G. W.; Martin, R. M. *J. Chem. Phys.* **1984**, *81*, 2352.
(11) de Vries, M. S.; Tyndall, G. W.; Cobb, C. L.; Martin, R. M. *J. Chem. Phys.* **1986**, *84*, 3753.
(12) Vredenbregt, E. J. D.; van Besouw, M. P. M.; Vrakking, M. J. J.; Mietus, M. J.; Gerrits, C. E. P.; Beijerinck, H. C. W. *J. Chem. Phys.* **1993**, *98*, 7903.
(13) Hennessy, R. J.; Simons, J. P. *Mol. Phys.* **1981**, *44*, 1027.
(14) Gundel, L. A.; Setser, D. W.; Clyne, M. A.; Coxon, J. A.; Nip, W. *J. Chem. Phys.* **1976**, *64*, 4390.
(15) Velazco, J. E.; Kolts, J. H.; Setser, D. W. *J. Chem. Phys.* **1976**, *65*, 3468.
(16) Velazco, J. E.; Kolts, J. H.; Setser, D. W.; Coxon, J. A. *Chem. Phys. Lett.* **1977**, *46*, 99.
(17) Velazco, J. E.; Kolts, J. H.; Setser, D. W. *J. Chem. Phys.* **1978**, *69*, 4357.
(18) Kolts, J. H.; Velazco, J. E.; Setser, D. W. *J. Chem. Phys.* **1979**, *71*, 1247.
(19) Lin, D.; Setser, D. W. *J. Phys. Chem.* **1985**, *89*, 1561.
(20) Sadeghi, N.; Cheaib, M.; Setser, D. W. *J. Chem. Phys.* **1989**, *90*, 219
(21) Fraites, J. L.; Winicur, D. H. *J. Chem. Phys.* **1976**, *64*, 89.
(22) Golde, M. F.; Kvaran, A. *J. Chem. Phys.* **1980**, *72*, 434.
(23) Hennessy, R. J.; Simons, J. P. *Chem. Phys. Lett.* **1980**, *75*, 43.
(24) Golde, M. F.; Poletti, R. A. *Chem. Phys. Lett.* **1981**, *80*, 22.
(25) Tamagaka, K.; Setser, D. W.; Kolts, J. H. *J. Chem. Phys.* **1981**, *74*, 4286.
(26) Liegel, J.; Spiegel, H.; Sauerbrey, R.; Langhoff, H. *J. Chem. Phys.* **1983**, *79*, 247.
(27) Liu, D.; Yu, Y. C.; Setser, D. W. *J. Chem. Phys.* **1984**, *81*, 5830.
(28) Balamuta, J.; Golde, M. F.; Moyle, A. M. *J. Chem. Phys.* **1985**, *82*, 3169.
(29) Johnson, K.; Simons, J. P.; Smith, P. A.; Washington, C.; Kvaran, A. *Mol. Phys.* **1986**, *75*, 255.
(30) Sobczynski, R.; Beaman, R.; Setser, D. W.; Sadeghi, N. *Chem. Phys. Lett.* **1989**, *154*, 349.
(31) Sekiya, N.; Nishimura, Y. *Chem. Phys. Lett.* **1990**, *175*, 6.
(32) Hartree, W. S.; Simons, J. P. *J. Chem. Soc., Faraday Trans.* **1990**, *86*, 11.
(33) Chen, X.; Setser, D. W. *J. Phys. Chem.* **1991**, *95*, 8473.
(34) Gu, Y.; Guo, J.; Liu, C.; Cao, D.; Cai, J. *Can. J. Chem.* **1991**, *69*, 100.
(35) Komatsu, H.; Kano, S. S.; Takuma, H.; Shimizu, T. *Jpn. T. Appl. Phys.* **1992**, *31*, 9280.
(36) Kwei, G. H.; Herschbach, D. R. *J. Chem. Phys.* **1969**, *51*, 1742.
(37) Kolts, J. H.; Setser, D. W. *J. Phys. Chem.* **1978**, *82*, 1766.
(38) Setser, D. W.; Dreiling, T. D.; Brashears Jr., H. C.; Kolts, J. H. *Faraday Discuss. Chem. Soc.* **1979**, *67*, 255.
(39) Krauss, M.; Liu, B. *Chem. Phys. Lett.* **1976**, *44*, 257. Hay, P. J.; Dunning, T. H., Jr. *J. Chem. Phys.* **1977**, *66*, 1306. Krauss, M. *J. Chem. Phys.* **1977**, *67*, 1712. Dunning, T. H., Jr.; Hay, P. J. *J. Chem. Phys.* **1978**, *69*, 134. Hay, P. J.; Wadt, W. R.; Dunning Jr., T. H. *Annu. Rev. Phys. Chem.* **1979**, *30*, 311, and references therein. Krauss, M.; Stevens, W. J.; Julienne, P. S. *J. Comput. Chem.* **1982**, *3*, 372.
(40) Dunning, T. H., Jr.; Hay, P. J. *J. Chem. Phys.* **1977**, *66*, 3767. Cohen, J. S.; Wadt, W. R.; Hay. P. J. *J. Chem. Phys.* **1979**, *71*, 2955. Langhoff, S. R. *J. Chem. Phys.* **1980**, *73*, 2379.
(41) Staemmler, V.; Jaquet, R. *Chem. Phys.* **1985**, *92*, 141.
(42) Foresman, J. B.; Head-Gordon, M.; Pople, J. A.; Frisch, M. J. *J. Phys. Chem.* **1992**, *96*, 135.
(43) Frisch, M. J.; Trucks, G. W.; Schlegel, H. B.; Gill, P. M. W.; Johnson, B. G.; Robb, M. A.; Cheseman, J. R.; Keith, T. A.; Petersson, G. A.; Montgomery, J. A.; Raghavachari, K.; Al-Laham, M. A.; Zekrzewski, V. G.; Ortiz, J. V.; Foresman, J. B.; Cioslowski, J.; Stefanov, A.; Nanayakkara, A.; Challacombe, M.; Peng, C. Y.; Ayala, P. Y.; Chen, W.; Wong, M. W.; Andres, J. L.; Replogle, E. S.; Gomperts, R.; Martin, R. L.; Fox, D. J.; Binkley, J. S.; Defrees, D. J.; Baker, J.; Stewart, J. J. P.; Head-Gordon, M.; Gonzalez, C.; Pople, J. A. *Gaussian 94*, Gaussian Inc.: Pittsburgh, PA, 1995.

(44) Ross, B. O. *Acc. Chem. Res.* **1999**, *32*, 137.
(45) Donovan, R. J.; Greenhill, P.; MacDonald, M. A.; Yencha, A. J.; Hartree, W. S.; Johnson, K.; Jouvet, C.; Kvaran, A.; Simons, J. P. *Faraday Discuss. Chem. Soc.* **1987**, *84*, 221.
(46) Raff, L. M.; Thompson, D. L. *The classical trajectory approach to reactive scattering* in: *Theory of chemical reaction dynamics*; CRC Press: Boca Raton, FL, 1985; Vol. III and references therein.
(47) Huxley, P.; Murrell, J. N. *J. Chem. Soc., Faraday Trans.* **1983**, *79*, 323.
(48) Golde, M. F.; Ho, Y. S.; Ogura, H. *J. Chem. Phys.* **1982**, *76*, 3535.
(49) Gilibert, M.; González, M.; Lucas, J. M.; Sayós, R.; Solé, A. Unpublished work.
(50) Hooper, D. G. Program 248, QCPE, Bloomington: Indiana University, 1974.
(51) Rettner, C. T.; Simons, J. P. *Faraday Discuss. Chem. Soc*. **1979**, *67*, 329.
(52) Levine, R. D.; Bernstein, R. B. *Molecular Reaction Dynamics and Chemical Reactivity*; Oxford University Press: Oxford, UK, 1987.
(53) Hartree, W. S.; Simons, J. P.; González-Ureña, A. *J. Chem. Soc., Faraday Trans.* **1990**, *86*, 17.
(54) Albertí, M.; Giménez, X.; Aguilar, A. *Chem. Phys.* **1994**, *189*, 677.
(55) Albertí, M.; Giménez, X.; Aguilar, A.; González Ureña, A. *Mol. Phys.* **1995**, *85*, 949.
(56) Albertí, M.; Giménez, X.; Aguilar, A.; González Ureña, A. *Mol. Phys*. **1998**, *93*, 389.
(57) The use of the CPOAM model was based on the generalized version developed in ref 54. In particular, the recoil energy and maximum reactant impact parameter constancy is not assumed, as it was done in previous versions of the model.[53] This is possible thanks to considering a specific analytical dependence for the integral cross section with energy, as well as a power series expansion for the reactant translational energy dependence on E'_{trans}.
(58) Baer, M. *J. Chem. Phys*. **1975**, *62*, 305.
(59) Sathyamurthy, N. *Chem. Rev.* **1983**, *83*, 601.
(60) Albertí, M.; Prieto, M.; Aguilar, A. *J. Chem. Soc., Faraday Trans.* **1992**, *88*, 1615.
(61) Baer, M. *J. Chem. Phys*. **1975**, *62*, 4545.
(62) (a) Muckerman, J. T. *J. Chem. Phys*. **1971**, *54*, 1155. (b) Johnston, G. W.; Kornweitz, H.; Schechter, I.; Persky, A.; Katz, B.; Bersohn, R.; Levine, R. D. *J. Chem. Phys*. **1991**, *94*, 2749. (c) Aoiz, F. J.; Bañares, L.; Herrero, V. J.; Sáez-Rábanos, V.; Stark, K.; Tanarro, I.; Werner, H. J.; *Chem. Phys. Lett*. **1996**, *262*, 175. (d) Zhang, D. H.; Lee, S.-Y.; Baer, M. *J. Chem. Phys*. **2000**, *112*, 9802.